Chinese Journal of Electronics
Vol.32, No.6, Nov. 2023

Overlay CR-NOMA Assisted Intelligent Transportation System Networks with Imperfect SIC and CEEs

LI Xingwang[1], GAO Xuesong[1], LIU Yingting[2,3,4], HUANG Gaojian[1], ZENG Ming[5], and QIAO Dawei[6]

(1. *Physics and Electronic Information Engineering, Henan Polytechnic University, Jiaozuo 454003, China*)

(2. *School of Electronic and Information Engineering, Lanzhou Jiaotong University, Lanzhou 730070, China*)

(3. *State Grid Gansu Electric Power Research Institute, Lanzhou 730070, China*)

(4. *School of Electronic Engineering, Beijing University of Posts and Telecommunications, Beijing 100876, China*)

(5. *Department of Electrical and Computer Engineering, Laval University, Quebec City QC G1V 0A6, Canada*)

(6. *School of Emergency Management, Henan Polytechnic University, Jiaozuo 454003, China*)

Abstract — With the development of the mobile communication and intelligent information technologies, the intelligent transportation systems driven by the sixth generation (6G) has many opportunities to achieve ultra-low latency and higher data transmission rate. Nonetheless, it also faces the great challenges of spectral resource shortage and large-scale connection. To solve the above problems, non-orthogonal multiple access (NOMA) and cognitive radio (CR) technologies have been proposed. In this regard, we study the reliable and ergodic performance of CR-NOMA assisted intelligent transportation system networks in the presence of imperfect successive interference cancellation (SIC) and non-ideal channel state information. Specifically, the analytical expressions of the outage probability (OP) and ergodic sum rate (ESR) are derived through a string of calculations. In order to gain more insights, the asymptotic expressions for OP and ESR at high signal-to-noise ratio (SNR) regimes are discussed. We verify the accuracy of the analysis by Monte Carlo simulations, and the results show: i) Imperfect SIC and channel estimation errors (CEEs) have negative impacts on the OP and ESR; ii) The OP decreases with the SNR increasing until convergence to a fixed constant at high SNR regions; iii) The ESR increases with increasing SNR and there exists a ceiling in the high SNR region.

Key words — Cognitive radio network, Ergodic rate, Imperfect successive interference cancellation, Non-orthogonal multiple access, Outage probability.

I. Introduction

As the key enabling technology of the future intelligent transportation systems (ITS), Internet-of-vehicles (IoV) will greatly promote the development of society towards intelligence and informatization [1], [2]. Generally, IoV communication includes vehicle-to-vehicle (V2V), vehicle-to-infrastructure (V2I) and the vehicle-to-person (V2P) [3]. With the rapid development of the sixth generation (6G) mobile communication, the IoV of ITS networks driven by 6G can achieve higher data transmissionrate,lowerlatencyandhigherquality-of-service (QoS) [4], [5]. However, it also faces great challenges, such as spectrum shortage and large-scale connections [6]. In order to effectively solve the above problems, some promising technologies have been proposed, such as non-orthogonal multiple access (NOMA) [7] and cognitive radio [8].

NOMA is considered as a key technology in 6G since it can improve the spectral efficiency and reduce the latency by serving massive devices in the same resource block (time/frequency/code) using power multiplexing [9]. Moreover, at the transmitting side, the transmitter allocates different power to different users according to their channel conditions and carries out superposition coding. At the receiving side, the signal is

Manuscript Received Apr. 12, 2022; Accepted June 28, 2022. This work was supported by the Key Project of Guizhou Science and Technology Support Program through Grant Guizhou Key Science and Support ([2021]-001), the Doctoral Fund of Henan Polytechnic University (B2022-2), the National Natural Science Foundation of China (62171146, 61861041), the Natural Science Foundation of Gansu Province of China (20JR5RA536, 20JR10RA095), and the Gansu Postdoctoral Research Funding Project.

 DOI:10.23919/cje.2022.00.071

detected through the successive interference cancelation (SIC) technology [10]. And specifically, NOMA can ensure fairness among the served users by allocating different users with different powers [11].

There are numerous excellent research focusing on the investigations of NOMA in wireless networks [12]–[18]. The authors in [12] proposed a general framework to evaluate a downlink NOMA system performance. The authors in [13] studied the reliable performance of a downlink NOMA system under the conditions of second-order statistics of channel state information (CSI). In [14], Lu *et al.* designed a multi-carrier NOMA system for video transmission to meet the growing demands for video services such as massive traffic and low latency. The authors in [15] investigated the performance of NOMA-enabled unmanned aerial vehicle (UAV) relay networks by deducing the outage probability (OP) and ergodic capacity for both amplify-and-forward (AF) and decode-and-forward (DF) relaying protocols at UAV. The authors in [16] studied the effective capacity of a reconfigurable intelligent surfaces aided NOMA system. Xu *et al.* [17] proposed a cognitive orthogonal frequency-division multiplexing-NOMA network to increase the system capacity. To support ultra-reliability, high throughput and multiple concurrent connections, reference [18] investigated the variation of the diversity order of OP relative to the transmit power in a hybrid automatic repeat request assisted NOMA system.

Cognitive radio (CR) is another promising technology to improve the frequency spectrum utilization [8], [19]. In the CR networks, the secondary network is allowed to selectively access the authorized frequency spectrum of the primary network to solve the problem of insufficient spectrum [20]. According to the spectrum access paradigms, interweave, underlay, overlay are the three most popular CR models [21]. In interweave model, the secondary user (SU) is allowed to access the authorized frequency bands only when primary user (PU) does not occupy it. Underlay cognitive radio allows the primary and secondary users to transmit messages simultaneously in the same frequency band, but the interference to the primary user needs to be less than a predefined value [22]. In overlay mode, the secondary network uses part of the energy to help the primary network transmit and obtain the right to access the authorized spectrum, and it improves the performance of the primary network while realizing the simultaneous transmission of the primary and secondary networks [23].

Scanning the technical literature of recent years, the performance of CR network was discussed in many literature since CR technology can mitigate the shortage of spectrum resources to a certain extent [24]–[28]. In [24], the authors derived the analytical expression of OP and ergodic rate (ER) so as to compare the throughput performance of CR networks based on interweave and underlay. In more detail, to maximize the throughput of SU, Wang *et al.*. [25] proposed a channel-and-sensing-aware channel access strategy for an interweave cognitive network. In [26], the authors discussed the influence of improper Gaussian signaling on the underlay CR network performance. The authors in [27] designed a novel scheme of spatial modulation in overlay CR network and analyzed the system performance by calculating average symbol error rate. The authors in [28] designed a scheme about optimal transmitting power for underlay CR network to minimize the average symbol error probability.

To address the challenges of the exponentially growing demand for mobile traffic [29], many researchers introduced the CR technology into the NOMA networks, see references [30]–[34]. Liu *et al.* [30] deduced the analytical expression of OP by means of stochastic geometry in order to characterize the reliable performance of the proposed CR-NOMA network. Wei *et al.* [31] deduced the analytical expressions of the secrecy sum rate to study the secrecy performance of a NOMA-enabled underlay CR network. The authors in [32] analyzed the performance of a NOMA assisted underlay CR network by deriving the analytical expression of pairwise error probability of SU. The authors in [33] proposed a novel spectrum sharing framework for multi-user CR-NOMA network to effectively improve the spectrum efficiency. In [34], the authors optimized the power allocation of the proposed spectrum leasing scheme for CR network so that the QoS of the primary network has been met while maximizing the performance of the secondary network.

Based on the above discussions, the existing studies are mostly conducted under ideal conditions. However, the actual communication process is generally carried out under the non-ideal conditions, such as imperfect successive interference cancellation (ipSIC) and non-ideal CSI. ipSIC is produced by channel state information unattainable, receiver performance limitation or synchronization errors, residual impairments and error propagation during transmission, etc. [35]–[40], and the channel estimation errors (CEEs) result in non-ideal CSI. Chen *et al.* [36] designed a novel algorithm to reduce the influence of ipSIC on the considered system performance. In [37], the authors investigated the reliable and ergodic performance of a multi-input multi-output (MIMO) interference networks under the condition of non-ideal CSI. Yang *et al.* [38] studied the effect of non-ideal CSI on secrecy performance of multi-user massive MIMO networks. The authors in [39] con-

sidered nonlinear multi-objective optimization problem under ipSIC in order to maximize the sum capacity and minimize the total transmit power under the constraint of QoS. Further, the authors in [40] analyzed the influence of ipSIC, non-ideal CSI and imperfect timing synchronization on a space time block code-based NOMA network simultaneously.

Although many researchers have conducted studies on NOMA, CR, imperfect SIC and non-ideal CSI, the joint impacts of the above factors on system performance are rarely studied. Sun *et al.* in [41] modeled a NOMA vehicular communication network, and deduced the analytical expression for the OP of the considered network. However, the non-ideal CSI, ipSIC and CR network were not involved. On the premise of ensuring quality-of-service, Xiao *et al* in [42] optimized transmission time and power control for the proposed radio-frequency-powered CR network to achieve maximum energy efficiency. Unfortunately, NOMA was not taken into consideration. The authors in [43] studied a CR-NOMA network and proposed a new dynamic power transmission scheme to guarantee the QoS of the considered system. The fly in the ointment was that non-ideal CSI has not been taken into account. Li *et al.* assessed the reliability and security of cooperative NOMA and non-cooperative NOMA systems by calculating secrecy outage probability and connection outage probability in [44]. However, ipSIC and non-ideal CSI were not taken into account. Luo *et al.* analyzed the performance of a cognitive NOMA system, and deduced the analytical expression of OP and throughput under high SNR regions in [45], but the non-ideal CSI was not considered. The authors in [46] analyzed and optimized the OP and throughput of the proposed underlay CR-NOMA in the presence of ipSIC. However, non-ideal CSI was not included. In [47], the authors proposed a CR assisted-NOMA network based on ITS and evaluated the reliability of the considered network by analyzing OP and throughput. Nonetheless, the ergodic performance of the network was not considered. The authors in [48] introduced wireless power transmission into CR-NOMA network to solve the challenges of energy consumption and large-scale connection in ITS. The fly in the ointment was that non-ideal CSI has not been mentioned.

In order to fill these bridges, considering CEEs and ipSIC, we introduce a NOMA-based overlay CR (OCR) ITS system. In the considered system, the SR utilizes the spectrum resources of the primary network to transmit its own information. In return, the SU acts as a relay to transmit the information of the primary network to the primary receivers. The main contributions of this paper are as following.

- We propose a novel NOMA-based OCR system for the ITS, which consists of a primary vehicle network and a secondary vehicle network. In the primary network, the primary transmitter sends superimposed information to both the primary and secondary receiving vehicles. In the secondary network, the secondary receiving vehicle receives their own information and acts as the relay of the primary network to transmit information to the primary receiving vehicles. Moreover, in order to make the work more realistic, we consider the CEEs and ipSIC. Specifically, two channel estimation models are considered: i) The CEEs is a fixed constant; ii) The CEEs is a function related to the SNR.
- We evaluate the reliability performance of the system under consideration by deducing the analytical expressions of the OP. In order to obtain more precise insights, the asymptotic expressions of the OP at high SNR regions are analyzed. The derivations show that increasing transmit SNR enhances the reliability of the consideration system and the OP exists an error floor because of the constant estimation error.
- The ergodic sum rate (ESR) of primary and secondary network are derived through a series of calculations to evaluate the ergodicity of the ITS system. In addition, the asymptotic expressions of ESR at high SNR regions are also performed. These results indicate that increasing SNR enhances the system ergodicity and the value of ESR tends to a constant at high SNR regime.

Here are some notations about this paper. $E(\cdot)$ stands for expectation operation. $\mathcal{CN}(\mu,\sigma^2)$ represents the complex Gaussian random variable with mean μ and variance σ^2. In addition, $F_X(\cdot)$ and $f_X(\cdot)$ denote the cumulative distribution function (CDF) and the probability dense function (PDF) respectively. $E_i(x)$ is the exponential distribution function, and can be expressed as $E_i(x)=\int_0^{\infty}\frac{e^{\rho}}{\rho}\mathrm{d}\rho$.

II. System Model

As illustrated in Fig.1, we consider a NOMA-based OCR system of ITS, which consists of a primary transmitter (PT), a marginal vehicle (PR1), a stronger vehicle (PR2) in primary network, a secondary transmitter (ST), and a secondary receiving vehicle (SR) in secondary network. It is assumed that: i) All nodes are equipped with one antenna; ii) All channels follow the independent Rayleigh fading.

It is difficult to obtain perfect CSI due to some practical factors, so the channel estimation method is introduced. By using linear minimum mean square error (LMMSE), the channel coefficient can be written as follows [49]:

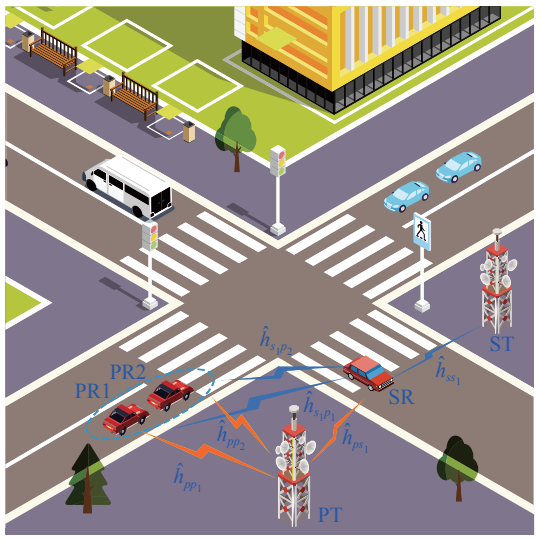

Fig. 1. System model.

$$h_i = \hat{h}_i + e_i \tag{1}$$

where $\hat{h}_i$ represents the estimated channel coefficient, $e_i \sim \mathcal{CN}(0, \sigma_{e_i}^2)$ represents the estimated error. $\hat{h}_i$ and e_i is independent and orthogonal because of the orthogonality of the LMMSE algorithm. The estimated channels are denoted as $\hat{h}_{pp_1} \sim \mathcal{CN}(0, \lambda_{pp_1})$, $\hat{h}_{pp_2} \sim \mathcal{CN}(0, \lambda_{pp_2})$, $\hat{h}_{ps_1} \sim \mathcal{CN}(0, \lambda_{ps_1})$, $\hat{h}_{ss_1} \sim \mathcal{CN}(0, \lambda_{ss_1})$, $\hat{h}_{s_1p_1} \sim \mathcal{CN}(0, \lambda_{s_1p_1})$, $\hat{h}_{s_1p_2} \sim \mathcal{CN}(0, \lambda_{s_1p_2})$.

As in [50], we consider two channel estimation models:

1) $\sigma_{e_i}^2$ is a fixed constant, which is independent of the average SNR.

2) $\sigma_{e_i}^2$ is a function associated with the average SNR and the expression is $\sigma_{e_i}^2 = \Omega_i/(1+\delta\gamma\Omega_i)$, where Ω_i is the variance of h_i, γ is the transmit SNR, while $\delta \geq 0$ represents the quality of channel estimation.

The whole communication process is divided into two slots.

1. The first slot

1) Received signals at PR1

PT transmits the superimposed signal to PR1, PR2 and SR through power domain multiplexing, and thus, the signal received at PR1 can be written as

$$y_{pp_1} = (\hat{h}_{pp_1} + e_{pp_1})(\sqrt{\alpha_1 P_p} x_{p,1} + \sqrt{\alpha_2 P_p} x_{p,2}) + n_{pp_1} \tag{2}$$

where $x_{p,1}$ and $x_{p,2}$ are the signals for PR1 and PR2 with $E(|x_{p,1}|^2) = 1$ and $E(|x_{p,2}|^2) = 1$. P_p is the transmit power of PT, α_1 and α_2 are the power allocation coefficients of the transmitting information $x_{p,1}$ and $x_{p,2}$ with satisfying $\alpha_1 + \alpha_2 = 1$, respectively. n_{pp_1} is the complex Gaussian noise and it follows $n_{pp_1} \sim \mathcal{CN}(0, N_n)$.

PR1 decodes $x_{p,1}$ and regards $x_{p,2}$ as a noise. The received signal-interference-plus-noise ratio (SINR) can be written as

$$\gamma_{x_{p,1}}^{pp_1} = \frac{\left|\hat{h}_{pp_1}\right|^2 \alpha_1 \rho_p}{\left|\hat{h}_{pp_1}\right|^2 \alpha_2 \rho_p + \sigma_{e_{pp_1}}^2 \rho_p + 1} \tag{3}$$

where $\rho_p = \frac{P_p}{N_n}$ is the transmit SINR at PT.

2) Received signals at PR2

The signal received in PR2 can be expressed as

$$y_{pp_2} = (\hat{h}_{pp_2} + e_{pp_2})(\sqrt{\alpha_1 P_p} x_{p,1} + \sqrt{\alpha_2 P_p} x_{p,2}) + n_{pp_2} \tag{4}$$

where $n_{pp_2} \sim \mathcal{CN}(0, N_n)$.

PR2 first decodes $x_{p,1}$ then decodes $x_{p,2}$ by using SIC on the basis of NOMA protocol. When decoding $x_{p,1}$, the SINR at PR2 can be represented as

$$\gamma_{x_{p,1}}^{pp_2} = \frac{\left|\hat{h}_{pp_2}\right|^2 \alpha_1 \rho_p}{\left|\hat{h}_{pp_2}\right|^2 \alpha_2 \rho_p + \sigma_{e_{pp_2}}^2 \rho_p + 1} \tag{5}$$

In practice, the receiver always have some types of errors in transmitting and detecting process, such as synchronization error, residual impairments or intrinsic constraints, therefore we assume ipSIC happens at PR2. The SINR of decoding $x_{p,2}$ at PR2 can be denoted by

$$\gamma_{x_{p,2}}^{pp_2} = \frac{\left|\hat{h}_{pp_2}\right|^2 \alpha_2 \rho_p}{\zeta_1 \left|\hat{h}_{pp_2}\right|^2 \alpha_1 \rho_p + \sigma_{e_{pp_2}}^2 \rho_p + 1} \tag{6}$$

where ζ_1 reprsents the coefficient of imperfect SIC and $0 \leq \zeta_1 \leq 1$. $\zeta_1 = 0$ and $\zeta_1 = 1$ indicate perfect SIC and no SIC, respectively.

3) Received signals at SR

The signal received at SR can be denoted as

$$y_{ps_1} = (\hat{h}_{ps_1} + e_{ps_1})(\sqrt{\alpha_1 P_p} x_{p,1} + \sqrt{\alpha_2 P_p} x_{p,2}) + n_{ps_1} \tag{7}$$

where $n_{pp_3} \sim \mathcal{CN}(0, N_n)$.

SR needs to decode the message $x_{p,1}$ of PR1 before decoding the message $x_{p,2}$ of PR2. The SINR of decoding $x_{p,1}$ and $x_{p,2}$ respectively at SR can be represented as

$$\gamma_{x_{p,1}}^{ps_1} = \frac{\left|\hat{h}_{ps_1}\right|^2 \alpha_1 \rho_p}{\left|\hat{h}_{ps_1}\right|^2 \alpha_2 \rho_p + \sigma_{e_{ps_1}}^2 \rho_p + 1} \tag{8}$$

$$\gamma_{x_{p,2}}^{ps_1} = \frac{\left|\hat{h}_{ps_1}\right|^2 \alpha_2 \rho_p}{\zeta_2 \left|\hat{h}_{ps_1}\right|^2 \alpha_1 \rho_p + \sigma_{e_{ps_1}}^2 \rho_p + 1} \tag{9}$$

where ζ_2 reprsents the coefficient of imperfect SIC and $0 \leq \zeta_2 \leq 1$.

2. The second slot

During the second slot, SR receives the message x_s from ST, while acting as a relay to decode and forward the messages $x_{p,1}$ and $x_{p,2}$ to PR1 and PR2[*1].

The two phases of receiving and decoding-and-forward the message are performed in the same resource block.

1) Received signals at SR

The signal received at SR can be written as

$$y_{ss_1} = (\hat{h}_{ss_1} + e_{ss_1})\sqrt{P_s}x_s + n_{ss_1} \tag{10}$$

where x_s denotes the message for SR with $E(|x_s|^2) = 1$, P_s represents the transmit power of ST, and $n_{ss_1} \sim \mathcal{CN}(0, N_n)$.

When decoding x_s, the SINR at SR can be expressed as

$$\gamma_{x_s}^{ss_1} = \frac{\left|\hat{h}_{ss_1}\right|^2 \rho_s}{\sigma_{e_{ss_1}}^2 \rho_s + 1} \tag{11}$$

where $\rho_s = \frac{P_s}{N_n}$ represents the transmit SINR of ST.

2) Received signals at PR1

The received signals at PR1 can be denoted by

$$y_{s_1p_1} = (\hat{h}_{s_1p_1} + e_{s_1p_1})(\sqrt{\alpha_3 P_{s_1}}x_{p,1} + \sqrt{\alpha_4 P_{s_1}}x_{p,2}) + n_{s_1p_1} \tag{12}$$

where $n_{s_1p_1} \sim \mathcal{CN}(0, N_n)$, P_{s_1} is the overall transmit power of SR, α_3 and α_4 are the power allocation coefficients of $x_{p,1}$ and $x_{p,2}$, respectively, and satisfying $\alpha_3 + \alpha_4 = 1$.

PR1 only decodes $x_{p,1}$ by considering other signals as interference. The SINR at PR1 can be computed as

$$\gamma_{x_{p,1}}^{s_1p_1} = \frac{\left|\hat{h}_{s_1p_1}\right|^2 \alpha_3 \rho_{s_1}}{\left|\hat{h}_{s_1p_1}\right|^2 \alpha_4 \rho_{s_1} + \sigma_{e_{s_1p_1}}^2 \rho_{s_1} + 1} \tag{13}$$

where $\rho_{s_1} = \frac{P_{s_1}}{N_n}$ represents the transmit SINR of SR.

3) Received signals at PR2

The received signals at PR2 can be represented as

$$y_{s_1p_2} = (\hat{h}_{s_1p_2} + e_{s_1p_2})(\sqrt{\alpha_3 P_{s_1}}x_{p,1} + \sqrt{\alpha_4 P_{s_1}}x_{p,2}) + n_{s_1p_2} \tag{14}$$

where $n_{s_1p_2} \sim \mathcal{CN}(0, N_n)$.

PR2 needs to decode the message $x_{p,1}$ of marginal user before decoding its own message $x_{p,2}$. Therefore, the SINR of decoding $x_{p,1}$ and $x_{p,2}$ at PR2 can be respectively computed as

$$\gamma_{x_{p,1}}^{s_1p_2} = \frac{\left|\hat{h}_{s_1p_2}\right|^2 \alpha_3 \rho_{s_1}}{\left|\hat{h}_{s_1p_2}\right|^2 \alpha_4 \rho_{s_1} + \sigma_{e_{s_1p_2}}^2 \rho_{s_1} + 1} \tag{15}$$

$$\gamma_{x_{p,2}}^{s_1p_2} = \frac{\left|\hat{h}_{s_1p_2}\right|^2 \alpha_4 \rho_{s_1}}{\zeta_3\left|\hat{h}_{s_1p_2}\right|^2 \alpha_3 \rho_{s_1} + \sigma_{e_{s_1p_2}}^2 \rho_{s_1} + 1} \tag{16}$$

where ζ_3 represents the coefficient of ipSIC, and it satisfies $0 \le \zeta_3 \le 1$.

III. Performance Analysis

The OP and ESR are the two important evaluation metrics of wireless communication systems. In this section, we study the reliability and ergodicity by calculating OP and ESR, and analyze the asymptotic expressions of OP and ESR at high SNR region.

1. Outage probability analysis

1) Outage probability for PR1

There are three conditions that the outage event occurs at PR1 according to the NOMA protocol: i) PR1 fails to decodes $x_{p,1}$ in direct link; ii) SR fails to decode the message $x_{p,1}$ and $x_{p,2}$ from PT; iii) SR decodes the $x_{p,1}$ and $x_{p,2}$ successfully, but PR1 cannot decode the message $x_{p,1}$ successfully. Therefore, the OP at PR1 can be computed as

$$\begin{aligned} P_{\text{out}}^{PR1} = &\left(1 - P_r\left(\gamma_{x_{p,1}}^{pp_1} > \gamma_{\text{th}1}\right)\right) \\ &\times \left(1 - P_r\left(\min\left(\frac{\gamma_{x_{p,1}}^{ps_1}}{\gamma_{\text{th}1}}, \frac{\gamma_{x_{p,2}}^{ps_1}}{\gamma_{\text{th}2}}, \frac{\gamma_{x_{p,1}}^{s_1p_1}}{\gamma_{\text{th}1}}\right) > 1\right)\right) \end{aligned} \tag{17}$$

where $\gamma_{\text{th}1}$ and $\gamma_{\text{th}2}$ is the target SINR of $x_{p,1}$ and $x_{p,2}$, respectively.

Theorem 1 The analytical expression of OP at PR1 is presented as

$$P_{\text{out}}^{PR1} = \left(1 - \mathrm{e}^{-\frac{M_1}{\lambda_{pp_1}}}\right)\left(1 - \mathrm{e}^{-\frac{M_4}{\lambda_{ps_1}} - \frac{M_5}{\lambda_{s_1p_1}}}\right) \tag{18}$$

if $0 < \gamma_{\text{th}1} < \min\left(\frac{\alpha_3}{\alpha_4}, \frac{\alpha_1}{\alpha_2}\right)$ and $0 < \gamma_{\text{th}2} < \frac{\alpha_2}{\zeta_2\alpha_1}$, otherwise P_{out}^{PR1} is equal to 1, where $M_1 = \frac{\gamma_{\text{th}1}(\sigma_{e_{pp_1}}^2\rho_p+1)}{\rho_p(\alpha_1-\alpha_2\gamma_{\text{th}1})}$, $M_2 = \frac{\gamma_{\text{th}1}(\sigma_{e_{ps_1}}^2\rho_p+1)}{\rho_p(\alpha_1-\alpha_2\gamma_{\text{th}1})}$, $M_3 = \frac{\gamma_{\text{th}2}(\sigma_{e_{ps_1}}^2\rho_p+1)}{\rho_p(\alpha_2-\zeta_2\alpha_1\gamma_{\text{th}2})}$, $M_4 = \max(M_2, M_3)$, and $M_5 = \frac{\gamma_{\text{th}1}(\sigma_{e_{s_1p_1}}^2\rho_{s_1}+1)}{\rho_{s_1}(\alpha_3-\alpha_4\gamma_{\text{th}1})}$.

Proof See Appendix A.

Corollary 1 At high SNRs ($\rho_p \to \infty$, $\rho_{s_1} \to \infty$), the OP approximate expression of PR1 can be expressed as

[*1]PT and ST can also send messages to SR at the same time, but the SR will cause interference, so this case is considered in this paper.

$$P_{\text{out},\infty}^{PR1}=\left(1-\mathrm{e}^{-\frac{M_6}{\lambda_{pp_1}}}\right)\left(1-\mathrm{e}^{-\frac{M_9}{\lambda_{ps_1}}-\frac{M_{10}}{\lambda_{s_1p_1}}}\right) \tag{19}$$

where $M_6=\frac{\gamma_{\text{th}1}\sigma_{e_{pp_1}}^2}{\alpha_1-\alpha_2\gamma_{\text{th}1}}$, $M_7=\frac{\gamma_{\text{th}1}\sigma_{e_{ps_1}}^2}{\alpha_1-\alpha_2\gamma_{\text{th}1}}$, $M_8=\frac{\gamma_{\text{th}2}\sigma_{e_{ps_1}}^2}{\alpha_2-\zeta_2\alpha_1\gamma_{\text{th}2}}$, $M_9=\max(M_7,M_8)$, and $M_{10}=\frac{\gamma_{\text{th}1}\sigma_{e_{s_1p_1}}^2}{\alpha_3-\alpha_4\gamma_{\text{th}1}}$.

2) Outage probability for PR2

There are three conditions when PR2 encounters outage event: i) PR2 cannot decodes $x_{p,1}$ and $x_{p,2}$ from the direct link successfully; ii) SR cannot decodes $x_{p,1}$ and $x_{p,2}$ from PT successfully; iii) SR decodes $x_{p,1}$ and $x_{p,2}$ from PT successfully, but PR2 fails to decode $x_{p,1}$ and $x_{p,2}$ from SR. Thus we can calculate the OP at PR2 as

$$\begin{aligned}P_{\text{out}}^{PR2}=&\left(1-P_r\left(\min\left(\frac{\gamma_{x_{p,1}}^{pp_2}}{\gamma_{\text{th}1}},\frac{\gamma_{x_{p,2}}^{pp_2}}{\gamma_{\text{th}2}}\right)>1\right)\right)\\&\times\left(1-P_r\left(\min\left(\frac{\gamma_{x_{p,1}}^{ps_1}}{\gamma_{\text{th}1}},\frac{\gamma_{x_{p,2}}^{ps_1}}{\gamma_{\text{th}2}},\frac{\gamma_{x_{p,1}}^{s_1p_2}}{\gamma_{\text{th}1}},\frac{\gamma_{x_{p,2}}^{s_1p_2}}{\gamma_{\text{th}2}}\right)>1\right)\right)\end{aligned} \tag{20}$$

Theorem 2 The analytical expression of OP at PR2 can be written as

$$P_{\text{out}}^{PR2}=\left(1-\mathrm{e}^{-\frac{M_{13}}{\lambda_{pp_2}}}\right)\left(1-\mathrm{e}^{-\frac{M_4}{\lambda_{ps_1}}-\frac{M_{16}}{\lambda_{s_1p_2}}}\right) \tag{21}$$

if $0<\gamma_{\text{th}1}<\min\left(\frac{\alpha_1}{\alpha_2},\frac{\alpha_3}{\alpha_4}\right)$ and $0<\gamma_{\text{th}2}<\min\left(\frac{\alpha_2}{\zeta_1\alpha_1},\frac{\alpha_4}{\zeta_2\alpha_3},\frac{\alpha_4}{\zeta_3\alpha_3}\right)$, otherwise P_{out}^{PR2} is equal to 1, where $M_{11}=\frac{\gamma_{\text{th}1}(\sigma_{e_{pp_2}}^2\rho_p+1)}{\rho_p(\alpha_1-\alpha_2\gamma_{\text{th}1})}$, $M_{12}=\frac{\gamma_{\text{th}2}(\sigma_{e_{pp_2}}^2\rho_p+1)}{\rho_p(\alpha_2-\zeta_1\alpha_1\gamma_{\text{th}2})}$, $M_{13}=\max(M_{11},M_{12})$, $M_{14}=\frac{\gamma_{\text{th}1}(\sigma_{e_{s_1p_2}}^2\rho_{s_1}+1)}{\rho_{s_1}(\alpha_3-\alpha_4\gamma_{\text{th}1})}$, $M_{15}=\frac{\gamma_{\text{th}2}(\sigma_{e_{s_1p_2}}^2\rho_{s_1}+1)}{\rho_{s_1}(\alpha_4-\zeta_3\alpha_3\gamma_{\text{th}2})}$, and $M_{16}=\max(M_{14},M_{15})$.

Proof See Appendix B.

Corollary 2 At high SNRs ($\rho_p\to\infty$, $\rho_{s_1}\to\infty$), the approximate expression of PR2 having outage event is

$$P_{\text{out},\infty}^{PR2}=\left(1-\mathrm{e}^{-\frac{M_{19}}{\lambda_{pp_2}}}\right)\left(1-\mathrm{e}^{-\frac{M_9}{\lambda_{ps_1}}-\frac{M_{22}}{\lambda_{s_1p_2}}}\right) \tag{22}$$

In (22), $M_{17}=\frac{\gamma_{\text{th}1}\sigma_{e_{pp_2}}^2}{\alpha_1-\alpha_2\gamma_{\text{th}1}}$, $M_{18}=\frac{\gamma_{\text{th}2}\sigma_{e_{pp_2}}^2}{\alpha_2-\zeta_1\alpha_1\gamma_{\text{th}2}}$, $M_{19}=\max(M_{17},M_{18})$, $M_{20}=\frac{\gamma_{\text{th}1}\sigma_{e_{s_1p_2}}^2}{\alpha_3-\alpha_4\gamma_{\text{th}1}}$, $M_{21}=\frac{\gamma_{\text{th}2}\sigma_{e_{s_1p_2}}^2}{\alpha_4-\zeta_3\alpha_3\gamma_{\text{th}2}}$, and $M_{22}=\max(M_{20},M_{21})$.

3) Outage probability for SR

The outage event will happen when SR fails to decode the message x_s, that is

$$P_{\text{out}}^{SR}=1-P_r(\gamma_{x_s}^{ss_1}>\gamma_{\text{ths}}) \tag{23}$$

where γ_{ths} represents the target SINR of decoding the message x_s.

Theorem 3 The analytical expression of OP at SR can be written as

$$P_{\text{out}}^{SR}=1-\mathrm{e}^{-\frac{M_{23}}{\lambda_{ss_1}}} \tag{24}$$

where $M_{23}=\frac{\gamma_{\text{ths}}(\sigma_{e_{ss_1}}^2\rho_s+1)}{\rho_s}$.

Proof See Appendix C.

Corollary 3 At high SNRs ($\rho_s\to\infty$), the approximate expression of SR having outage event is

$$P_{\text{out},\infty}^{SR}=1-\mathrm{e}^{-\frac{\gamma_{\text{ths}}\sigma_{e_{ss_1}}^2}{\lambda_{ss_1}}} \tag{25}$$

To gain further insight, we discuss the diversity order of PR1, PR2 and SR. According to [7], the diversity order is defined as

$$d=-\lim_{\rho\to\infty}\frac{\log\left(P_{\text{out},\infty}\right)}{\log\rho} \tag{26}$$

Corollary 4 The diversity orders of PR1, PR2 and SR can be represent as

$$d_{PR1}=d_{PR2}=d_{SR}=0 \tag{27}$$

Remark 1 From **Corollary 1**, **Corollary 2** and **Corollary 3**, we can find that when the transmitted SNR approaches infinity, the asymptotic OPs of PR1, PR2 and SR become a fixed constant, indicating that the OP has an error floor, yielding the diversity order to be 0.

2. Ergodic sum rate analysis

1) Ergodic sum rate for primary network

The ESR of primary network can be expressed as

$$R_p=R_{PR1}+R_{PR2} \tag{28}$$

The ergodic rates (ERs) for PR1 and PR2 are inferred as follows.

2) Ergodic rate for PR1

The ER of PR1 can be written as

$$R_{PR1}=E\left[\frac{1}{2}\log_2(1+W)\right] \tag{29}$$

where $W=\min(u_1,u_2,u_3)$, $u_1=\gamma_{x_{p,1}}^{pp_1}$, $u_2=\gamma_{x_{p,1}}^{ps_1}$, and $u_3=\gamma_{x_{p,1}}^{s_1p_1}$.

Theorem 4 The analytical expression of ER at PR1 can be written as

$$R_{PR1}=\frac{1}{2\ln 2}\frac{\pi N}{2k}\sum_{i=0}^{k}\frac{2\sqrt{1-\phi_i^2}}{2+N(\phi_i+1)}e^{-M_{28}-M_{29}-M_{30}} \tag{30}$$

where $\phi_i=\cos\left(\frac{(2i-1)\pi}{2k}\right)$, $M_{25}=\frac{w(\sigma_{e_{pp_1}}^2\rho_p+1)}{\lambda_{pp_1}\rho_p(\alpha_1-w\alpha_2)}$, $M_{26}=\frac{w(\sigma_{e_{ps_1}}^2\rho_p+1)}{\lambda_{ps_1}\rho_p(\alpha_1-w\alpha_2)}$, $M_{27}=\frac{w(\sigma_{e_{s_1p_1}}^2\rho_{s_1}+1)}{\lambda_{s_1p_1}\rho_{s_1}(\alpha_3-w\alpha_4)}$, $M_{28}=\frac{N(\phi_i+1)(\sigma_{e_{pp_1}}^2\rho_p+1)}{\lambda_{pp_1}\rho_p(2\alpha_1-\alpha_2N(\phi_i+1))}$, $M_{29}=\frac{N(\phi_i+1)(\sigma_{e_{ps_1}}^2\rho_p+1)}{\lambda_{ps_1}\rho_p(2\alpha_1-\alpha_2N(\phi_i+1))}$

and $M_{30}=\frac{N(\phi_i+1)(\sigma^2_{e_{s_1p_1}}\rho_{s_1}+1)}{\lambda_{s_1p_1}\rho_{s_1}(2\alpha_3-\alpha_4N(\phi_i+1))}$.

Proof See Appendix D.

Corollary 5 At high SNRs ($\rho_p\to\infty$, $\rho_{s_1}\to\infty$), we can calculate the ER asymptotic expression of PR1 as

$$R^{\infty}_{PR_1}=\frac{1}{2\ln 2}\frac{\pi N}{2k}\sum_{i=0}^{k}\frac{2\sqrt{1-\phi_i{}^2}}{2+N(\phi_i+1)}e^{-M_{31}-M_{32}-M_{33}} \tag{31}$$

where $M_{31}=\frac{N(\phi_i+1)\sigma^2_{e_{pp_1}}}{\lambda_{pp_1}(2\alpha_1-\alpha_2N(\phi_i+1))}$, $M_{32}=\frac{N(\phi_i+1)\sigma^2_{e_{ps_1}}}{\lambda_{ps_1}(2\alpha_1-\alpha_2N(\phi_i+1))}$ and $M_{33}=\frac{N(\phi_i+1)\sigma^2_{e_{s_1p_1}}}{\lambda_{s_1p_1}(2\alpha_3-\alpha_4N(\phi_i+1))}$.

3) Ergodic rate for PR2

The ER of PR2 can be represented as

$$R_{PR2}=E\left[\frac{1}{2}\log_2(1+Z)\right] \tag{32}$$

where $Z=\min(v_1,v_2,v_3)$, $v_1=\gamma^{pp_2}_{x_{p,2}}$, $v_2=\gamma^{ps_1}_{x_{p,2}}$, and $v_3=\gamma^{s_1p_2}_{x_{p,2}}$.

Theorem 5 The analytical expression of ER at PR2 is given by

$$R_{PR2}=\frac{1}{2\ln 2}\frac{\pi N_2}{2k}\sum_{i=0}^{k}\frac{2\sqrt{1-\phi_i{}^2}}{2+N_2(\phi_i+1)}\mathrm{e}^{-M_{37}-M_{38}-M_{39}} \tag{33}$$

where $M_{34}=\frac{z(\sigma^2_{e_{pp_2}}\rho_p+1)}{\lambda_{pp_2}\rho_p(\alpha_2-z\zeta_1\alpha_1)}$, $M_{35}=\frac{z(\sigma^2_{e_{ps_1}}\rho_p+1)}{\lambda_{ps_1}\rho_p(\alpha_2-z\zeta_2\alpha_1)}$, $M_{36}=\frac{z(\sigma^2_{e_{s_1p_2}}\rho_{s_1}+1)}{\lambda_{s_1p_2}\rho_{s_1}(\alpha_4-z\zeta_3\alpha_3)}$, $M_{37}=\frac{N_2(\phi_i+1)(\sigma^2_{e_{pp_2}}\rho_p+1)}{\lambda_{pp_2}\rho_p(2\alpha_2-\alpha_1N_2(\phi_i+1)\zeta_1)}$, $M_{38}=\frac{N_2(\phi_i+1)(\sigma^2_{e_{ps_1}}\rho_p+1)}{\lambda_{ps_1}\rho_p(2\alpha_2-\alpha_1N_2(\phi_i+1)\zeta_2)}$ and M_{39} is expressed as $M_{39}=\frac{N_2(\phi_i+1)(\sigma^2_{e_{s_1p_2}}\rho_{s_1}+1)}{\lambda_{s_1p_2}\rho_{s_1}(2\alpha_4-\alpha_3N_2(\phi_i+1)\zeta_3)}$.

Proof See Appendix E.

Corollary 6 At high SNRs ($\rho_p\to\infty$, $\rho_{s_1}\to\infty$), we can calculate the ER asymptotic expression of PR2 as

$$R^{\infty}_{PR2}=\frac{1}{2\ln 2}\frac{\pi N_2}{2k}\sum_{i=0}^{k}\frac{2\sqrt{1-\phi_i{}^2}}{2+N_2(\phi_i+1)}\mathrm{e}^{-M_{40}-M_{41}-M_{42}} \tag{34}$$

where M_{40} and M_{41} are $M_{40}=\frac{N_2(\phi_i+1)\sigma^2_{e_{pp_2}}}{\lambda_{pp_2}(2\alpha_2-\alpha_1N_2(\phi_i+1)\zeta_1)}$ and $M_{41}=\frac{N_2(\phi_i+1)\sigma^2_{e_{ps_1}}}{\lambda_{ps_1}(2\alpha_2-\alpha_1N_2(\phi_i+1)\zeta_2)}$, respectively, M_{42} is $M_{42}=\frac{N_2(\phi_i+1)\sigma^2_{e_{s_1p_2}}}{\lambda_{s_1p_2}(2\alpha_4-\alpha_3N_2(\phi_i+1)\zeta_3)}$.

Theorem 6 The ESR of primary network can be expressed as

$$R_p=\frac{\pi}{4\ln 2}\left(\frac{N}{k}\sum_{i=0}^{k}\frac{2\sqrt{1-\phi_i{}^2}}{2+N(\phi_i+1)}\mathrm{e}^{-M_{28}-M_{29}-M_{30}}+\frac{N_2}{k}\sum_{i=0}^{k_2}\frac{2\sqrt{1-\phi_i{}^2}}{2+N_2(\phi_i+1)}\mathrm{e}^{-M_{37}-M_{38}-M_{39}}\right) \tag{35}$$

Corollary 7 At high SNRs ($\rho_s\to\infty$), we can simplify the ESR asymptotic expression of primary network as

$$R^{\infty}_{P}=\frac{\pi}{4\ln 2}\left(\frac{N}{k}\sum_{i=0}^{k}\frac{2\sqrt{1-\phi_i{}^2}}{2+N(\phi_i+1)}\mathrm{e}^{-M_{31}-M_{32}-M_{33}}+\frac{N_2}{k}\sum_{i=0}^{k}\frac{2\sqrt{1-\phi_i{}^2}}{2+N_2(\phi_i+1)}\mathrm{e}^{-M_{40}-M_{41}-M_{42}}\right) \tag{36}$$

4) Ergodic sum rate for secondary network

The ESR of secondary network can be expressed as

$$R_S=E\left[\frac{1}{2}\log_2(1+\gamma^{ss_1}_{x_s})\right] \tag{37}$$

Theorem 7 The ESR of secondary network is given by

$$R_S=-\frac{1}{2\ln 2}\mathrm{e}^{-\frac{(\sigma^2_{e_{ss_1}}\rho_s+1)}{\lambda_{ss_1}\rho_s}}E_i\left(-\frac{(\sigma^2_{e_{ss_1}}\rho_s+1)}{\lambda_{ss_1}\rho_s}\right) \tag{38}$$

Proof See Appendix F.

Corollary 8 At high SNRs ($\rho_s\to\infty$), we can simplify the ESR asymptotic expression of secondary network as

$$R^{\infty}_{S}=-\frac{1}{2\ln 2}\mathrm{e}^{-\frac{\sigma^2_{e_{ss_1}}}{\lambda_{ss_1}}}E_i\left(-\frac{\sigma^2_{e_{ss_1}}+1}{\lambda_{ss_1}}\right) \tag{39}$$

Remark 2 From **Corollary 7** and **Corollary 8**, we found that when the transmitted SNR approaches infinity, the asymptotic ESRs of primary network and secondary network become a fixed constant, implying that there exists a ceiling for ESR due to CEEs.

IV. Numerical Results and Discussion

In this section, we offer some numerical results to verify the correctness of the analysis in Section III, and these results are obtained based on the 10^6 Mente Carlo simulations. Unless otherwise specified, the parameter values are set as in Table 1.

Fig.2 shows the OP curves of the users under the ideal and non-ideal conditions. For the purpose of comparison, the parameter settings under the ideal conditions are provided, and the variances of CEEs are $\sigma^2_{e_{pp_1}}=\sigma^2_{e_{pp_2}}=\sigma^2_{e_{ps_1}}=\sigma^2_{e_{ss_1}}=\sigma^2_{e_{s_1p_1}}=\sigma^2_{e_{s_1p_2}}=0$. With

Table 1. Parameters for numerical results

Channel estimation error	$\sigma^2_{e_{pp_1}} = \sigma^2_{e_{pp_2}} = \sigma^2_{e_{ps_1}} = \sigma^2_{e_{ss_1}} = \sigma^2_{e_{s_1p_1}} = \sigma^2_{e_{s_1p_2}} = 0.01$
Estimated channel coefficient	$\{\lambda_{pp_1}, \lambda_{pp_2}, \lambda_{ps_1}, \lambda_{ss_1}, \lambda_{s_1p_1}, \lambda_{s_1p_2}\} = \{0.1, 0.5, 2, 0.1, 4, 3\}$
Power allocation coefficient	$\alpha_1 = \alpha_3 = 0.9 \quad \alpha_2 = \alpha_4 = 0.1$
Noise power	$N_n = 1$
Imperfect SIC	$\{\zeta_1, \zeta_2, \zeta_3\} = 0.001$
Targeted date rate	$\{\gamma_{\text{th}1}, \gamma_{\text{th}2}, \gamma_{\text{ths}}\} = \{1, 1, 2\}$

transmit SNR increasing, the OPs of PR1, PR2, SR decrease gradually and finally converge to fixed values, which leads to error floors. This means that when there are CEEs, the transmit power is not always beneficial to the reliable performance. Under ideal conditions, the OPs decrease with the SNR. In addition, the OP value of each user under the ideal condition is smaller than that under the non-ideal condition. This indicates that the existence of ipSIC and CEEs reduce the reliability of the system.

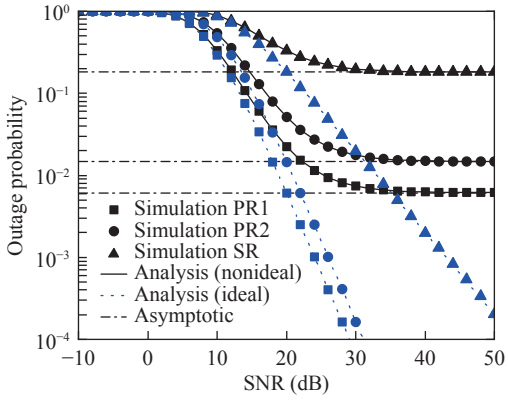

Fig. 2. The OP of the users in ideal and non-ideal conditions.

Fig.3 provides the curves of OP versus SNR under two channel estimation models: i) the channel estimation error is a fixed constant; ii) the channel estimation error is a function of the SNR. As can be seen from Fig.3, the theoretical analysis curves are in consistence

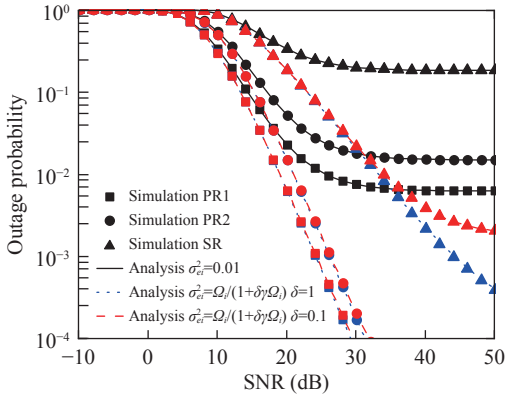

Fig. 3. The OP of the users in different channel estimation error models.

with the simulation results, validating the accuracy of our analysis. For the first model, the OP is a fixed constant in the high SNR regimes, while for the second mode, the OP decrease as the SNR grows large. This is because that when the SNR grows large, the estimated channel gradually approaches the real channel, yielding improves reliable performance.

Fig.4 plots the OPs of users versus power allocation parameter α_2 for different target rates. It is clear that the OP first decreases and then increases with α_2, we can draw the conclusion from equations (18) and (21). Fig.4 also indicates that when the target rates γ_{th1} and γ_{th2} are smaller, the OP of the considered system is smaller and the reliability of the system is higher. In addition, the optimal value of OP is insensitive to the target rates γ_{th1} and γ_{th2}.

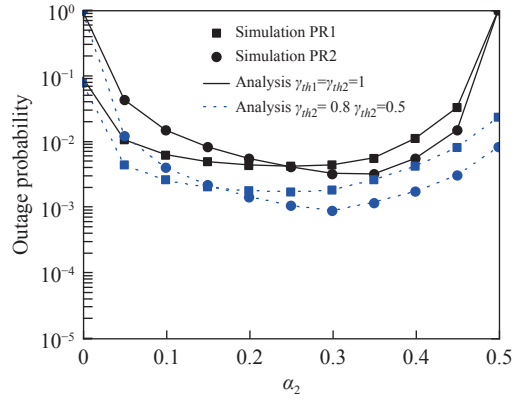

Fig. 4. OP versus α_2 for different γ_{th1}, γ_{th2}.

Fig.5 shows the ESR versus SNR. We set $N = 8$, $N_2 = 100$, and $k = k_2 = 100$. From Fig.5, we can observe that the ESR increases gradually with the SNR and then tends to a fixed constant under the non-ideal condition. In contrast, under the ideal condition ($\sigma^2_{e_{pp_1}} = \sigma^2_{e_{pp_2}} = \sigma^2_{e_{ps_1}} = \sigma^2_{e_{ss_1}} = \sigma^2_{e_{s_1p_1}} = \sigma^2_{e_{s_1p_2}} = 0$ and $\zeta_1 = \zeta_2 = \zeta_3 = 0$), the ESR grows linearly with the SNR. At high SNR regions, the analytical and asymptotic values of the ESR are basically coincident.

Fig.6 represents the relationship between ESR and transmitting SNR under the above mentioned two CEEs models. In this simulation, we set $N = 8$, $N_2 = 100$, $k = k_2 = 100$ and $\delta = \{0.1, 1\}$. we can see from Fig.6 that the ESR has a ceiling at high SNR regions when estimation error is a fixed constant, and the

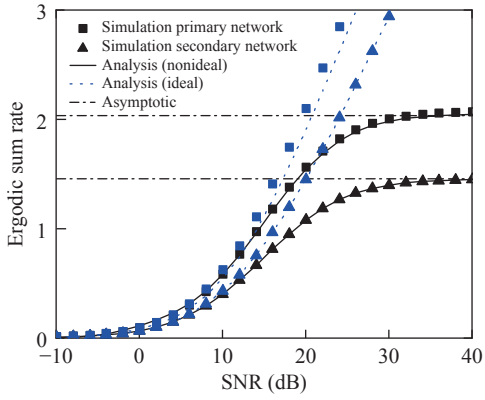

Fig. 5. The ESR under ideal and non-ideal condition.

ESR decreases with δ when the estimation error is a unary function. Changes in δ have a negligible effect on the system ESR value in the low SNR region.

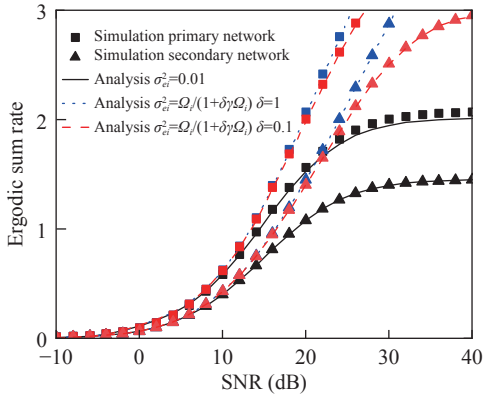

Fig. 6. The ESR in different channel estimation error models.

The relationship between ER and α_2 under different SNRs is depicted in Fig.7. In simulation, we set $N=8$, $N_2=100$, $k=k_2=100$ and SNR $=\{10,15\}$ dB. The ER of PR1 decreases as the power allocation parameter α_2 increases, while the ER of PR2 increases with α_2, which can be inferred from equations (30) and (33). Generally speaking, the larger α_2 is, the easier to decode $x_{p,2}$ and the more difficult to decode $x_{p,1}$. That is, the combination of $x_{p,1}$ and $x_{p,2}$ could explain the changes in the curves.

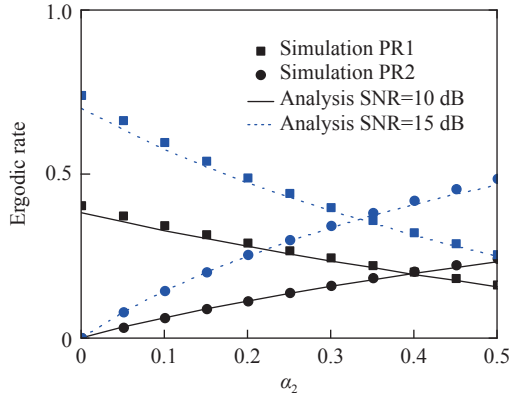

Fig. 7. Ergodic Rate versus α_2 for different SNR.

V. Conclusions

To improve the spectral efficiency, we proposed a NOMA-based OCR system for ITS. The reliability and ergodicity of the proposed system were analyzed by considering ipSIC and two channel estimation models. We derived the analytical expressions of the OP and ESR, as well as the asymptotic expressions of OP and ESR at the high SNR region. A series of simulations were carried out to verify the accuracy of the analysis. In addition, the effect of a series of related parameters on the system performance were investigated through simulation.

Appendix A. Proof of Theorem 1

The proof starts by substituting equations (3), (8), (9), (13) into (17), the OP for PR1 can be written as

$$P_{\text{out}}^{PR1}=\underbrace{\left(1-P_r\left(\gamma_{x_{p,1}}^{pp_1}>\gamma_{th1}\right)\right)}_{I_1}\times\underbrace{\left(1-P_r\left(\min\left(\frac{\gamma_{x_{p,1}}^{ps_1}}{\gamma_{th1}},\frac{\gamma_{x_{p,2}}^{ps_1}}{\gamma_{th2}},\frac{\gamma_{x_{p,1}}^{s_1p_1}}{\gamma_{th1}}\right)>1\right)\right)}_{I_2} \tag{A-1}$$

where I_1 and I_2 are calculated as follows:

$$\begin{aligned}I_1&=1-P_r\left(\gamma_{x_{p,1}}^{pp_1}>\gamma_{th1}\right)\\&=1-P_r\left(\left|\hat{h}_{pp_1}\right|^2>M_1\right)\\&=1-\mathrm{e}^{-\frac{M_1}{\lambda_{pp_1}}}\end{aligned} \tag{A-2}$$

and

$$\begin{aligned}I_2&=1-P_r\left(\min\left(\frac{\gamma_{x_{p,1}}^{ps_1}}{\gamma_{th1}},\frac{\gamma_{x_{p,2}}^{ps_1}}{\gamma_{th2}},\frac{\gamma_{x_{p,1}}^{s_1p_1}}{\gamma_{th1}}\right)>1\right)\\&=1-P_r\left(\gamma_{x_{p,1}}^{ps_1}>\gamma_{th1},r_{x_{p,2}}^{ps_1}>\gamma_{th2},\gamma_{x_{p,1}}^{s_1p_1}>\gamma_{th1}\right)\\&=1-P_r\left(\left|\hat{h}_{ps_1}\right|^2>M_2,\left|\hat{h}_{ps_1}\right|^2>M_3,\left|\hat{h}_{s_1p_1}\right|^2>M_5\right)\\&=1-P_r\left(\left|\hat{h}_{ps_1}\right|^2>M_4,\left|\hat{h}_{s_1p_1}\right|^2>M_5\right)\\&=1-\mathrm{e}^{-\frac{M_4}{\lambda_{ps_1}}-\frac{M_5}{\lambda_{s_1p_1}}}\end{aligned} \tag{A-3}$$

Appendix B. Proof of Theorem 2

The proof starts by substituting equations (5), (6), (8), (9), (15), (16) into (20), the OP for PR2 can be written as

$$P_{\text{out}}^{PR2}=\underbrace{\left(1-P_r\left(\min\left(\frac{\gamma_{x_{p,1}}^{pp_2}}{\gamma_{th1}},\frac{\gamma_{x_{p,2}}^{pp_2}}{\gamma_{th2}}\right)>1\right)\right)}_{I_3}\times\underbrace{\left(1-P_r\left(\min\left(\frac{\gamma_{x_{p,1}}^{ps_1}}{\gamma_{th1}},\frac{\gamma_{x_{p,2}}^{ps_1}}{\gamma_{th2}},\frac{\gamma_{x_{p,1}}^{s_1p_2}}{\gamma_{th1}},\frac{\gamma_{x_{p,2}}^{s_1p_2}}{\gamma_{th2}}\right)>1\right.\right.}_{I_4} \tag{B-1}$$

where I_3 and I_4 are calculated as follows:

$$\begin{aligned}I_3&=1-P_r\left(\min\left(\frac{\gamma_{x_{p,1}}^{pp_2}}{\gamma_{th1}},\frac{\gamma_{x_{p,2}}^{pp_2}}{\gamma_{th2}}\right)>1\right)\\&=1-P_r\left(\gamma_{x_{p,1}}^{pp_2}>\gamma_{th1},\gamma_{x_{p,2}}^{pp_2}>\gamma_{th2}\right)\\&=1-P_r\left(\left|\hat{h}_{pp_2}\right|^2>M_{11},\left|\hat{h}_{pp_2}\right|^2>M_{12}\right)\\&=1-P_r\left(\left|\hat{h}_{pp_2}\right|^2>M_{13}\right)\\&=1-\mathrm{e}^{-\frac{M_{13}}{\lambda_{pp_2}}}\end{aligned} \tag{B-2}$$

and

$$\begin{aligned}I_4&=1-P_r\left(\min\left(\frac{\gamma_{x_{p,1}}^{ps_1}}{\gamma_{th1}},\frac{\gamma_{x_{p,2}}^{ps_1}}{\gamma_{th2}},\frac{\gamma_{x_{p,1}}^{s_1p_2}}{\gamma_{th1}},\frac{\gamma_{x_{p,2}}^{s_1p_2}}{\gamma_{th2}}\right)>1\right)\\&=1-P_r\left(\gamma_{x_{p,1}}^{ps_1}>\gamma_{th1},\gamma_{x_{p,2}}^{ps_1}>\gamma_{th2},\gamma_{x_{p,1}}^{s_1p_2}>\gamma_{th1},\gamma_{x_{p,2}}^{s_1p_2}>\right.\\&=1-\mathrm{e}^{-\frac{M_4}{\lambda_{ps_1}}}P_r\left(\left|\hat{h}_{s_1p_2}\right|^2>M_{14},\left|\hat{h}_{s_1p_2}\right|^2>M_{15}\right)\\&=1-\mathrm{e}^{-\frac{M_4}{\lambda_{ps_1}}}P_r\left(\left|\hat{h}_{s_1p_2}\right|^2>M_{16}\right)\\&=1-\mathrm{e}^{-\frac{M_4}{\lambda_{ps_1}}-\frac{M_{16}}{\lambda_{s_1p_2}}}\end{aligned} \tag{B-3}$$

Appendix C. Proof of Theorem 3

The proof starts by substituting equation (11) into (23), the OP for SR can be written as

$$\begin{aligned}P_{\text{out}}^{SR}&=1-P_r\left(\gamma_{x_s}^{ss_1}>\gamma_{ths}\right)\\&=1-P_r\left(\left|\hat{h}_{ss_1}\right|^2>M_{23}\right)\\&=1-\mathrm{e}^{-\frac{M_{23}}{\lambda_{ss_1}}}\end{aligned} \tag{C-1}$$

Appendix D. Proof of Theorem 4

Based on the definition of expectation, equation (28) can be further calculated as

$$R_{PR_1}=E\left[\frac{1}{2}\log_2(1+W)\right]=\frac{1}{2\ln 2}\int_0^{+\infty}\frac{1-F_W(w)}{1+w}\mathrm{d}w \tag{D-1}$$

It is assumed that $f_W(w)$, $F_W(w)$ are the PDF and CDF of random variable W respectively. $F_W(w)$ can be computed as

$$\begin{aligned}F_W(w)&=P_r(W<w)=P_r(\min(u_1,u_2,u_3)<w)\\&=1-P_r(\min(u_1,u_2,u_3)>w)\\&=1-P_r(u_1>w,u_2>w,u_3>w)\\&=1-\mathrm{e}^{-M_{25}-M_{26}-M_{27}}\end{aligned} \tag{D-2}$$

We can figure out the ER of PR1 by plugging (D-2) into (D-1),

$$\begin{aligned}R_{PR_1}&=\frac{1}{2\ln 2}\int_0^{+\infty}\frac{1-F_W(w)}{1+w}\mathrm{d}w\\&=\frac{1}{2\ln 2}\int_0^{+\infty}\frac{1}{1+w}\mathrm{e}^{-M_{25}-M_{26}-M_{27}}\mathrm{d}w\end{aligned} \tag{D-3}$$

It is difficult to acquire an accurate closed-formed solution. Alternatively, we obtain the approximation with the aid of Gaussian-Chebyshev quadrature as [51]

$$\begin{aligned}R_{PR_1}&=\frac{1}{2\ln 2}\int_0^{+\infty}\frac{1}{1+w}\mathrm{e}^{-M_{25}-M_{26}-M_{27}}\mathrm{d}w\\&\approx\frac{1}{2\ln 2}\int_0^{N}\frac{1}{1+w}\mathrm{e}^{-M_{25}-M_{26}-M_{27}}\mathrm{d}w\\&=\frac{1}{2\ln 2}\frac{\pi N}{2k}\sum_{i=0}^{k}\frac{2\sqrt{1-\phi_i^2}}{2+N(\phi_i+1)}\mathrm{e}^{-M_{28}-M_{29}-M_{30}}\end{aligned} \tag{D-4}$$

Appendix E. Proof of Theorem 5

It is assumed that $F_Z(z)$ is the CDF of random variable Z. We can obtain the expression by calculating as follows:

$$\begin{aligned}F_Z(z)&=P_r(Z<z)=P_r(\min(v_1,v_2,v_3)<z)\\&=1-P_r(v_1>z,v_2>z,v_3>z)\\&=1-\mathrm{e}^{-M_{34}-M_{35}-M_{36}}\end{aligned} \tag{E-1}$$

The ER of PR2 can be written as

$$\begin{aligned}R_{PR_2}&=\frac{1}{2\ln 2}\int_0^{+\infty}\frac{1-F_Z(z)}{1+z}\mathrm{d}z\\&=\frac{1}{2\ln 2}\int_0^{+\infty}\frac{1}{1+z}\mathrm{e}^{-M_{34}-M_{35}-M_{36}}\mathrm{d}z\end{aligned} \tag{E-2}$$

Since exact closed-formed expressions are not available, considering that when N_2 is a large number, we have the following equation according to Gaussian-Chebyshev quadrature.

$$\begin{aligned}R_{PR_2}&=\frac{1}{2\ln 2}\int_0^{+\infty}\frac{1}{1+z}\mathrm{e}^{-M_{34}-M_{35}-M_{36}}\mathrm{d}z\\&\approx\frac{1}{2\ln 2}\int_0^{N_2}\frac{1}{1+z}\mathrm{e}^{-M_{34}-M_{35}-M_{36}}\mathrm{d}z\\&=\frac{1}{2\ln 2}\frac{\pi N_2}{2k_2}\sum_{i=0}^{k_2}\frac{2\sqrt{1-\phi_i^2}}{2+N_2(\phi_i+1)}\mathrm{e}^{-M_{37}-M_{38}-M_{39}}\end{aligned} \tag{E-3}$$

Appendix F. Proof of Theorem 7

Letting $\theta=r_{x_s}^{ss_1}$ to facilitate the calculation, we can obtain the PDF of θ as

$$F_\theta(\theta) = P_r\left(\frac{\left|\hat{h}_{ss_1}\right|^2\rho_s}{\sigma^2_{e_{ss_1}}\rho_s+1} < \theta\right) = P_r\left(\left|\hat{h}_{ss_1}\right|^2 < \frac{\theta(\sigma^2_{e_{ss_1}}\rho_s+1)}{\rho_s}\right) = \mathrm{e}^{-\frac{\theta(\sigma^2_{e_{ss_1}}\rho_s+1)}{\lambda_{ss_1}\rho_s}} \quad \text{(F-1)}$$

By inserting (F-1) into (37), equation (38) can be acquired.

$$R_S = E\left[\frac{1}{2}\log_2(1+\gamma^{ss_1}_{x_s})\right] = \frac{1}{2\ln 2}\int_0^\infty \frac{1-F_\theta(\theta)}{1+\theta}\mathrm{d}\theta = \frac{1}{2\ln 2}\int_0^\infty \frac{1}{1+\theta}\mathrm{e}^{-\frac{\theta(\sigma^2_{e_{ss_1}}\rho_s+1)}{\lambda_{ss_1}\rho_s}}\mathrm{d}\theta = -\frac{1}{2\ln 2}\mathrm{e}^{-\frac{(\sigma^2_{e_{ss_1}}\rho_s+1)}{\lambda_{ss_1}\rho_s}}E_i\left(-\frac{(\sigma^2_{e_{ss_1}}\rho_s+1)}{\lambda_{ss_1}\rho_s}\right) \quad \text{(F-2)}$$

References

[1] J. H. Zhao, X. K. Sun, Q. P. Li, *et al.*, "Edge caching and computation management for real-time internet of vehicles: an online and distributed approach," *IEEE Transactions on Intelligent Transportation Systems*, vol.22, no.4, pp.2183–2197, 2021.

[2] H. H. Yang, J. C. Shang , J. J. Li, *et al.*, "Multi-traffic targets tracking based on an improved structural sparse representation with spatial-temporal constraint," *Chinese Journal of Electronics*, vol.31, no.2, pp.266–276, 2022.

[3] Y. K. Zheng, X. W. Li, H. Zhang, *et al.*, "Overlay cognitive ABCom-NOMA-Based ITS: an in-depth secrecy analysis," *IEEE Transactions on Intelligent Transportation Systems*, vol.24, no.2, pp.2217–2228, 2023.

[4] M. Y. Wang, Y. Lin, Q. Tian, *et al.*, "Transfer learning promotes 6G wireless communications: recent advances and future challenges," *IEEE Transactions on Reliability*, vol.70, no.2, pp.790–807, 2021.

[5] G. Y. Liu, Y. H. Huang, N. Li, *et al.*, "Vision, requirements and network architecture of 6G mobile network beyond 2030," *China Communications*, vol.17, no.9, pp.92–104, 2020.

[6] M. Chen and Y. Q. Yang, "Iterative interference cancellation for non-orthogonal multiple access system," *Chinese Journal of Electronics*, vol.29, no.3, pp.540–546, 2020.

[7] Z. G. Ding, P. Z. Fan, G. K. Karagiannidis, *et al.*, "NOMA assisted wireless caching: strategies and performance analysis," *IEEE Transactions on Communications*, vol.66, no.10, pp.4854–4876, 2018.

[8] Z. Y. Xu, Z. G. Sun , L. L. Guo, *et al.*, "Joint spectrum sensing and spectrum access for defending massive SSDF attacks: A novel defense framework," *Chinese Journal of Electronics*, vol.31, no.2, pp.240–254, 2022.

[9] Y. Z. Tan and B. R. Chen, "Joint channel estimation and power allocation for the CRS-NOMA," *Chinese Journal of Electronics*, vol.29, no.1, pp.177–182, 2020.

[10] S. Arzykulov, T. A. Tsiftsis, G. Nauryzbayev, *et al.*, "Outage performance of cooperative underlay CR-NOMA with imperfect CSI," *IEEE Communications Letters*, vol.23, no.1, pp.176–179, 2019.

[11] L. Bai, L. N. Zhu, Q. Yu, *et al.*, "Transmit power minimization for vector-perturbation based NOMA Systems: a suboptimal beamforming approach," *IEEE Transactions on Wireless Communications*, vol.18, no.5, pp.2679–2692, 2019.

[12] M. S. Van Nguyen, D. T. Do, S. Al-Rubaye, *et al.*, "Exploiting impacts of antenna selection and energy harvesting for massive network connectivity," *IEEE Transactions on Communications*, vol.69, no.11, pp.7587–7602, 2021.

[13] Z. Yang, Z. G. Ding, P. Z. Fan, *et al.*, "On the performance of non-orthogonal multiple access systems with partial channel information," *IEEE Transactions on Communications*, vol.64, no.2, pp.654–667, 2016.

[14] H. C. Lu, X. D. Jiang, and C. W. Chen, "Distortion-aware cross-layer power allocation for video transmission over multi-user NOMA systems," *IEEE Transactions on Wireless Communications*, vol.20, no.2, pp.1076–1092, 2021.

[15] D. T. Do, A. T. Le, Y. W. Liu, *et al.*, "User grouping and energy harvesting in UAV-NOMA system with AF/DF relaying," *IEEE Transactions on Vehicular Technology*, vol.70, no.11, pp.11855–11868, 2021.

[16] G. Li, H. L. Liu, G. J. Huang, *et al.*, "Effective capacity analysis of reconfigurable intelligent surfaces aided NOMA network," *EURASIP Journal on Wireless Communications and Networking*, vol.2021, no.1, article no.198, 2021.

[17] W. J. Xu, X. Li, C. H. Lee, *et al.*, "Joint sensing duration adaptation, user matching, and power allocation for cognitive OFDM-NOMA Systems," *IEEE Transactions on Wireless Communications*, vol.17, no.2, pp.1269–1282, 2018.

[18] Z. Shi, C. M. Zhang, Y. R. Fu, *et al.*, "Achievable diversity order of HARQ-Aided downlink NOMA systems," *IEEE Transactions on Vehicular Technology*, vol.69, no.1, pp.471–487, 2020.

[19] F. Lin, Z. Hu, S. J. Hou, *et al.*, "Cognitive radio network as wireless sensor network (II): security consideration," in *Proceedings of 2011 IEEE National Aerospace and Electronics Conference*, Dayton, OH, USA, pp.324–328, 2011.

[20] H. Li, W. J. Zhao, C. Liu, *et al.*, "A novel goodness of fit test spectrum sensing using extreme eigenvalues," *Chinese Journal of Electronics*, vol.29, no.6, pp.1201–1206, 2020.

[21] S. Singh and M. Bansal,, "On the outage performance of overlay cognitive STBC-NOMA system with imperfect SIC," *IEEE Wireless Communications Letters*, vol.10, no.11, pp.2587–2591, 2021.

[22] P. Das and N. B. Mehta, "Direct link-aware optimal relay selection and a low feedback variant for underlay CR," *IEEE Transactions on Communications*, vol.63, no.6, pp.2044–2055, 2015.

[23] X. W. Li, Y. K. Zheng, M. D. Alshehri, *et al.*, "Cognitive AmBC-NOMA IoV-MTS networks with IQI: reliability and security analysis," *IEEE Transactions on Intelligent Transportation Systems*, vol.24, no.2, pp.2596–2607, 2023.

[24] M. C. Filippou, D. Gesbert, and G. A. Ropokis, "A comparative performance analysis of interweave and underlay multi-antenna cognitive radio networks," *IEEE Transactions on Wireless Communications*, vol.14, no.5, pp.2911–2925, 2015.

[25] S. H. Wang, C. Y. Hsu, and Y. W. P. Hong, "Distributed exploitation of spectrum and channel state information for channel reservation and selection in interweave cognitive radio networks," *IEEE Transactions on Wireless Communications*, vol.12, no.7, pp.3458–3472, 2013.

[26] C. Lameiro, I. Santamaría, P. J. Schreier, *et al.*, "Maximally improper signaling in underlay MIMO cognitive radio

networks," *IEEE Transactions on Signal Processing*, vol.67, no.24, pp.6241–6255, 2019.

[27] A. Alizadeh, H. R. Bahrami, and M. Maleki, "Performance analysis of spatial modulation in overlay cognitive radio communications," *IEEE Transactions on Communications*, vol.64, no.8, pp.3220–3232, 2016.

[28] S. Kashyap and N. B. Mehta, "SEP-optimal transmit power policy for peak power and interference outage probability constrained underlay cognitive radios," *IEEE Transactions on Wireless Communications*, vol.12, no.12, pp.6371–6381, 2013.

[29] J. H. Zhao, S. J. Ni, L. H. Yang, *et al.*, "Multiband cooperation for 5G HetNets: a promising network paradigm," *IEEE Vehicular Technology Magazine*, vol.14, no.4, pp.85–93, 2019.

[30] Y. W. Liu, Z. G. Ding, M. Elkashlan, *et al.*, "Nonorthogonal multiple access in large-scale underlay cognitive radio networks," *IEEE Transactions on Vehicular Technology*, vol.65, no.12, pp.10152–10157, 2016.

[31] L. W. Wei, T. Jing, X. Fan, *et al.*, "The secrecy analysis over physical layer in NOMA-enabled cognitive radio networks," in *Proceedings of 2018 IEEE International Conference on Communications*, Kansas City, MO, USA, pp.1–6, 2018.

[32] L. Bariah, S. Muhaidat, and A. Al-Dweik, "Error performance of NOMA-based cognitive radio networks with partial relay selection and interference power constraints," *IEEE Transactions on Communications*, vol.68, no.2, pp.765–777, 2020.

[33] L. Lv, L. Yang, H. Jiang, *et al.*, "When NOMA meets multiuser cognitive radio: opportunistic cooperation and user scheduling," *IEEE Transactions on Vehicular Technology*, vol.67, no.7, pp.6679–6684, 2018.

[34] A. H. Bastami, "NOMA-based spectrum leasing in cognitive radio network: power optimization and performance analysis," *IEEE Transactions on Communications*, vol.69, no.7, pp.4821–4831, 2021.

[35] H. F. Shuai, K. F. Guo, K. An, *et al.*, "NOMA-based integrated satellite terrestrial networks with relay selection and imperfect SIC," *IEEE Access*, vol.9, pp.111346–111357, 2021.

[36] X. M. Chen, R. D. Jia, and D. W. K. Ng, "On the design of massive non-orthogonal multiple access with imperfect successive interference cancellation," *IEEE Transactions on Communications*, vol.67, no.3, pp.2539–2551, 2019.

[37] X. M. Chen and C. Yuen, "On interference alignment with imperfect CSI: characterizations of outage probability, Ergodic rate and SER," *IEEE Transactions on Vehicular Technology*, vol.65, no.1, pp.47–58, 2016.

[38] T. H. Yang, R. Q. Zhang, X. Cheng, *et al.*, "Secure massive MIMO under imperfect CSI: performance analysis and channel prediction," *IEEE Transactions on Information Forensics and Security*, vol.14, no.6, pp.1610–1623, 2019.

[39] W. U. Khan, X. W. Li, A. Ihsan, *et al.*, "NOMA-enabled optimization framework for next-generation small-cell IoV networks under imperfect SIC decoding," *IEEE Transactions on Intelligent Transportation Systems*, vol.23, no.11, pp.22442–22451, 2022.

[40] M. W. Akhtar, S. A. Hassan, S. Saleem, *et al.*, "STBC-aided cooperative NOMA with timing offsets, imperfect successive interference cancellation, and imperfect channel state information," *IEEE Transactions on Vehicular Technology*, vol.69, no.10, pp.11712–11727, 2020.

[41] Y. S. Sun, Z. G. Ding, and X. C. Dai, "On the outage performance of network NOMA (N-NOMA) modeled by Poisson line cox point process," *IEEE Transactions on Vehicular Technology*, vol.70, no.8, pp.7936–7950, 2021.

[42] H. Xiao, H. Jiang, F. R. Shi, *et al.*, "Energy-efficient resource allocation in radio-frequency-powered cognitive radio network for connected vehicles," *IEEE Transactions on Intelligent Transportation Systems*, vol.22, no.8, pp.5426–5436, 2021.

[43] Z. Yang, J. A. Hussein, P. Xu, *et al.*, "Performance study of cognitive relay NOMA networks with dynamic power transmission," *IEEE Transactions on Vehicular Technology*, vol.70, no.3, pp.2882–2887, 2021.

[44] B. Li, X. H. Qi, K. Z. Huang, *et al.*, "Security-reliability tradeoff analysis for cooperative NOMA in cognitive radio networks," *IEEE Transactions on Communications*, vol.67, no.1, pp.83–96, 2019.

[45] L. P. Luo, Q. Z. Li, and J. L. Cheng, "Performance analysis of overlay cognitive NOMA systems with imperfect successive interference cancellation," *IEEE Transactions on Communications*, vol.68, no.8, pp.4709–4722, 2020.

[46] A. V. and B. A. V., "Performance analysis of NOMA-based underlay cognitive radio networks with partial relay selection," *IEEE Transactions on Vehicular Technology*, vol.70, no.5, pp.4615–4630, 2021.

[47] D. T. Do, T. A. Le, T. N. Nguyen, *et al.*, "Joint impacts of imperfect CSI and imperfect SIC in cognitive radio-assisted NOMA-V2X communications," *IEEE Access*, vol.8, pp.128629–128645, 2020.

[48] D. T. Do, M. S. van Nguyen, M. Voznak, *et al.*, "Performance analysis of clustering car-following V2X system with wireless power transfer and massive connections," *IEEE Internet of Things Journal*, vol.9, no.16, pp.14610–14628, 2022.

[49] X. W. Li, Q. S. Wang, M. Liu, *et al.*, "Cooperative wireless-powered NOMA relaying for B5G IoT networks with hardware impairments and channel estimation errors," *IEEE Internet of Things Journal*, vol.8, no.7, pp.5453–5467, 2021.

[50] X. W. Li, J. J. Li, Y. W. Liu, *et al.*, "Residual transceiver hardware impairments on cooperative NOMA networks," *IEEE Transactions on Wireless Communications*, vol.19, no.1, pp.680–695, 2020.

[51] Q. Q. Zhang, L. Zhang, Y. C. Liang, *et al.*, "Backscatter-NOMA: a symbiotic system of cellular and internet-of-things networks," *IEEE Access*, vol.7, pp.20000–20013, 2019.

LI Xingwang received the M.S. and Ph.D. degrees from University of Electronic Science and Technology of China and Beijing University of Posts and Telecommunications in 2010 and 2015, respectively. From 2010 to 2012, he worked as an Engineer at Comba Telecom Ltd. in Guangzhou, China. From 2017 to 2018, he was a Visiting Scholar at Queen's University Belfast, Belfast, UK. He is also a Visiting Scholar at State Key Laboratory of Networking and Switching Technology, Beijing University of Posts and Telecommunications from 2016 to 2018. He is currently an Associated Professor with the School of Physics and Electronic Information Engineering, Henan Polytechnic University, Jiaozuo, China. His research interests include MIMO communication, cooperative communication, hardware constrained communication, non-orthogonal multiple access, physical layer security, unmanned aerial vehicles, and the Internet of things. He has served as many TPC members, such as IEEE GLOBECOM'18, IEEE WCNC'20, IEEE VTC'20,

IEEE ICCC'19 and so on. He has also served as the Co-Chair for the IEEE/IET CSNDSP'20 and IEEE PIMRC'21. He also serves as an Editor on the Editorial Boards of *IEEE Transactions on Vehicular Technology*, *IEEE Systems Journal*, *IEEE Access*, *Computer Communications*, *IET Networks*, *Physical Communication*, *IET Quantum Communication*, and *KSII Transactions on Internet and Information Systems*. He is also the Lead Guest Editor for the Special Issue on UAV-Enabled B5G/6Gnetworks: Emerging Trends and Challenges of *Physical Communication*, Special Issue on Recent Advances in Physical Layer Technologies for the 5G-Enabled Internet of Things of *Wireless Communications and Mobile Computing*, and Special Issue on Recent Advances in Multiple Access for 5G-Enabled IoT of *Security and Communication Networks*. (Email: lixingwangbupt@gmail.com)

GAO Xuesong received the B.S. degree in information engineering with the School of Physics and Information Engineering of Cangzhou Normal University, Cangzhou, China, in 2021. She is currently pursuing the M.S. degree in communication and information systems with the School of Physics and Electronic Information Engineering, Henan Polytechnic University, Jiaozuo, China. Her current research interests include non-orthogonal multiple access, cognitive radio, and cooperative communication. (Email: gaoxuesong@home.hpu.edu.cn)

LIU Yingting received the B.S., M.S. and Ph.D. degrees, all in communication & information systems, from Xidian University in 2005, 2008 and 2012, respectively. From 2012 to 2015, he was a Senior Engineer of Information and Communication Company of Gansu Power Corporation. From 2016 to 2021, he was serving as an Associate Professor in Northwest Normal University. Now, he is serving as an Associate Professor with the School of Electronic and Information Engineering, Lanzhou Jiaotong University. His research mainly focuses on some hot fields in wireless communications, e.g., simultaneously wireless information and power transfer, non-orthogonal multiple assess and backscatter communications. Moreover, the performance optimization for the communication system is also his research interests. (Email: liuyt2018@163.com)

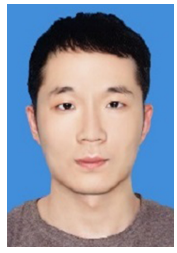

HUANG Gaojian received the B.S. degree in electronic information engineering from the Guilin University of Electronic Technology (GUET), Guilin, China, in 2013, and received the Ph.D. degree in information and communications engineering from GUET, in 2021. From October 2017 to October 2018, he was a Visiting Researcher at Queen's University Belfast, Northern Ireland, UK. He is now a Lecturer at the School of Physics and Electronic Information Engineering, Henan Polytechnic University, Jiaozuo, China. His research interests include integrated sensing and wireless communication designs, antenna array, physical layer security, emerging modulation techniques and 5G/6G related areas. (Email: g.huang@hpu.edu.cn)

ZENG Ming received the B.E. and M.S. degrees from Beijing University of Post and Telecommunications, China in 2013 and 2016, respectively, and the Ph.D. degree in telecommunications engineering from Memorial University, Canada, in 2020. Currently, he is an Assistant Professor at the Department of Electrical Engineering and Computer Engineering, Université Laval, Canada. He has published more than 45 articles and conferences in first-tier IEEE journals and proceedings, and his work has been cited over 1150 times per Google Scholar. His research interests include resource allocation for beyond 5G systems, and machine learning empowered optical communications. He serves as an Associate Editor of the *IEEE Open Journal of the Communication Society*. (Email: ming.zeng@gel.ulaval.ca)

QIAO Dawei received the B.S. degree in public management with the School of Medicine, Henan Polytechnic University, Jiaozuo, China, in 2021. Before this, she worked at the Hospital of Henan Polytechnic University from 2015 to 2018. Her current research interests include artificial intelligence, health management, e-health and Internet of medical things. (Email: daweihpu@163.com)